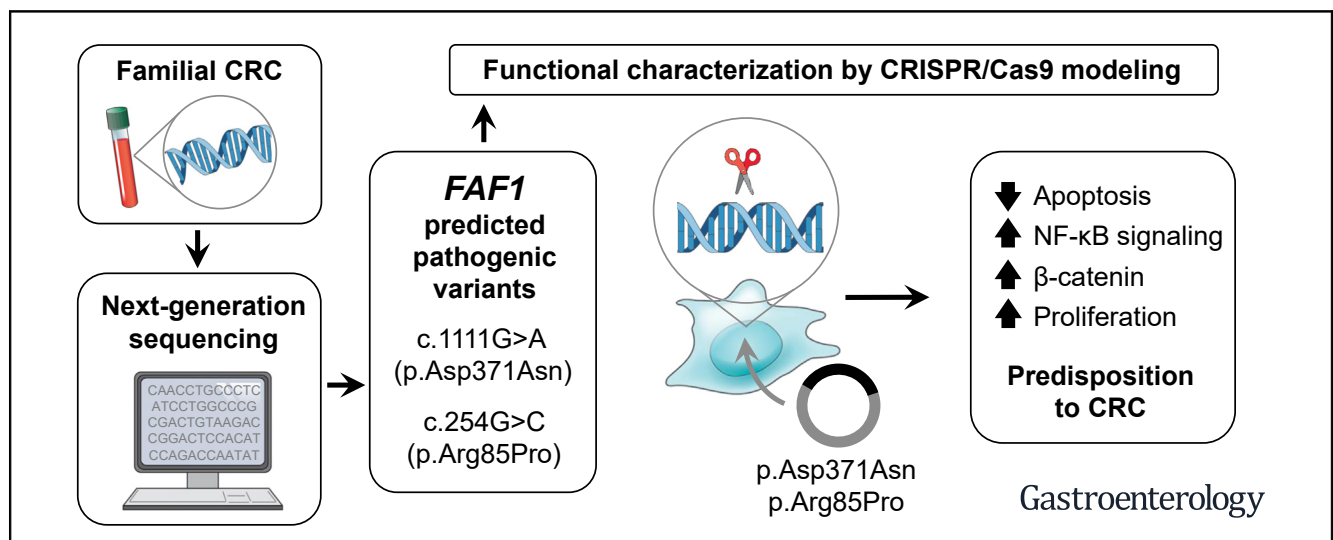




# Germline Mutations in *FAF1* Are Associated With Hereditary Colorectal Cancer

Laia Bonjoch,<sup>1</sup> Sebastià Franch-Expósito,<sup>1</sup> Pilar Garre,<sup>2</sup> Sami Belhadj,<sup>3</sup> Jenifer Muñoz,<sup>1</sup> Coral Arnau-Collell,<sup>1</sup> Marcos Díaz-Gay,<sup>1</sup> Anna Gratacós-Mulleras,<sup>1</sup> Giulia Raimondi,<sup>4</sup> Clara Esteban-Jurado,<sup>1</sup> Yasmin Soares de Lima,<sup>1</sup> Cristina Herrera-Pariente,<sup>1</sup> Miriam Cuatrecasas,<sup>5</sup> Teresa Ocaña,<sup>1</sup> Antoni Castells,<sup>1</sup> Cristina Fillat,<sup>4</sup> Gabriel Capellá,<sup>3</sup> Francesc Balaguer,<sup>1</sup> Trinidad Caldés,<sup>2</sup> Laura Valle,<sup>3</sup> and Sergi Castellví-Bel<sup>1</sup>

<sup>1</sup>Gastroenterology Department, Institut d'Investigacions Biomèdiques August Pi i Sunyer (IDIBAPS), Centro de Investigación Biomédica en Red de Enfermedades Hepáticas y Digestivas (CIBEREHD), Hospital Clínic, Universitat de Barcelona, Barcelona, Spain; <sup>2</sup>Molecular Oncology Laboratory, Centro Investigación Biomédica en Red de Cáncer (CIBERONC), Hospital Clínico San Carlos, Instituto de Investigación Sanitaria San Carlos (IdISSC), Madrid, Spain; <sup>3</sup>Hereditary Cancer Program, Catalan Institute of Oncology, Oncobell, Institut d'Investigació Biomèdica de Bellvitge (IDIBELL), Centro de Investigación Biomédica en Red de Cáncer (CIBERONC), Barcelona, Spain; <sup>4</sup>Gene Therapy and Cancer, Institut d'Investigacions Biomèdiques August Pi i Sunyer (IDIBAPS), Centro de Investigación Biomédica en Red de Enfermedades Raras (CIBERER), Universitat de Barcelona, Barcelona, Spain; and <sup>5</sup>Pathology Department, Institut d'Investigacions Biomèdiques August Pi i Sunyer (IDIBAPS), Centro de Investigación Biomédica en Red de Enfermedades Hepáticas y Digestivas (CIBEREHD) and Tumor Bank-Biobank, Hospital Clínic, Barcelona, Spain



**BACKGROUND & AIMS:** A significant proportion of colorectal cancer (CRC) cases have familial aggregation but little is known about the genetic factors that contribute to these cases. We performed an exhaustive functional characterization of genetic variants associated with familial CRC. **METHODS:** We performed whole-exome sequencing analyses of 75 patients from 40 families with a history of CRC (including early-onset cases) of an unknown germline basis (discovery cohort). We also sequenced specific genes in DNA from an external replication cohort of 473 families, including 488 patients with colorectal tumors that had normal expression of mismatch repair proteins (validation cohort). We disrupted the Fas-associated factor 1 gene (*FAF1*) in DLD-1 CRC cells using CRISPR/Cas9 gene editing; some cells were transfected with plasmids that express *FAF1* missense variants. Cells were analyzed by immunoblots, quantitative real-time polymerase chain reaction, and functional assays monitoring apoptosis, proliferation, and assays for Wnt signaling or nuclear factor (NF)-kappa-B

activity. **RESULTS:** We identified predicted pathogenic variant in the *FAF1* gene (c.1111G>A; p.Asp371Asn) in the discovery cohort; it was present in 4 patients of the same family. We identified a second variant in *FAF1* in the validation cohort (c.254G>C; p.Arg85Pro). Both variants encoded unstable *FAF1* proteins. Expression of these variants in CRC cells caused them to become resistant to apoptosis, accumulate beta-catenin in the cytoplasm, and translocate NF-kappa-B to the nucleus. **CONCLUSIONS:** In whole-exome sequencing analyses of patients from families with a history of CRC, we identified variants in *FAF1* that associate with development of CRC. These variants encode unstable forms of *FAF1* that increase resistance of CRC cells to apoptosis and increase activity of beta-catenin and NF-kappa-B.

**Keywords:** Wnt Signaling; Programmed Cell Death; Gene Editing; Functional Genomics.

Colorectal cancer (CRC) is one of the most frequent neoplasms worldwide, accounting for approximately 8% of all cancer-related deaths.<sup>1</sup> A familial component, defined by the presence of 2 or more affected relatives, is estimated to be involved in 12% to 35% of all CRC cases.<sup>2,3</sup> However, only 5.2% of all CRC cases are caused by known high-penetrance CRC genes (*APC*, *MUTYH*, the DNA polymerases *POLE* and *POLD1*, and the mismatch repair genes *MLH1*, *MSH2*, *MSH6*, and *PMS2*).<sup>4</sup> Despite these hereditary syndromic forms, a large proportion of patients with CRC have a family history of the disease but the underlying germline cause remains unexplained. Part of this familial risk could be related to uncommon and highly penetrant mutations in genes yet to be discovered. Numerous genes involved in CRC and/or polyposis predisposition have been proposed, although, so far, strong evidence of association has only been demonstrated for *NTHL1*, *MSH3*, *GREM1*, *RNF43*, *RSP20*, and *MLH3*.<sup>5-8</sup>

In the past years, genome-wide next-generation sequencing and copy-number technologies have been widely used for the identification of new germline variants involved in cancer predisposition. Nevertheless, recognizing the correct causal pathogenic variant among the large number of variants identified by using these genome-wide techniques is not straightforward. The functional characterization of the identified variants is a helpful approach to establish the link to disease predisposition. To standardize and facilitate this approach, key guidelines<sup>9,10</sup> and experimental scanning pipelines<sup>11,12</sup> have been developed to assess the functional relevance of the genetic variants. On the other hand, CRISPR/Cas gene editing has transformed functional genomics, enabling researchers to potentially edit any desired region of the genome. Modeling by CRISPR/Cas has allowed the characterization of several known hereditary CRC genes (eg, *MLH1* and *POLE*), as well as somatic CRC mutational events (*KRAS*, *TP53*, *SMAD4*, and *APC*).<sup>13,14</sup> Undoubtedly, the integration of next-generation sequencing results with these models can help monitor the genomic changes that trigger CRC development and allow more personalized therapy designs. Nevertheless, these cancer modeling tools have been scarcely used to decipher the pathogenicity of many variants of uncertain significance.

In this study, we aimed at identifying novel causal genes for CRC germline predisposition by performing whole-exome sequencing in CRC families with an unknown germline basis. The detected rare variants were functionally evaluated to demonstrate their pathogenicity and implications in predisposing to CRC, permitting a more accurate and adequate diagnosis of patients, as well as facilitating genetic counseling and prevention.

## Materials and Methods

### Patients

We selected 75 patients from 40 families with strong CRC aggregation where other known hereditary cancer syndromes had been ruled out (unaffiliated) and compatible with an autosomal dominant pattern of inheritance. The selection

### WHAT YOU NEED TO KNOW

#### BACKGROUND AND CONTEXT

Next-generation sequencing is frequently used to identify genetic variants associated with familial colorectal cancer (CRC). Studies are then needed to analyze the functional effects of these variants.

#### NEW FINDINGS

Using next-generation sequencing, the authors identified variants in *FAF1* carried by members of 2 families with histories of CRC and early-onset CRC. CRC cells with disruption of *FAF1*, or that overexpressed the variants identified in the cohorts, became resistant to apoptosis and had increased cytosolic beta-catenin and nuclear NF-kappa-B.

#### LIMITATIONS

Additional studies, of larger cohorts, are needed to determine how *FAF1* variants contribute to hereditary CRC. Studies of colon organoids are needed to determine how these variants affect colon tissues.


#### IMPACT

The combination of next-generation sequencing and functional analysis of identified disease-associated variants is an effective strategy to identify mechanisms of pathogenesis. It might be used to identify specific mechanisms of disease development in individual patients or families.

criteria were as follows: 3 or more relatives with CRC, 2 or more consecutive affected generations, and at least 1 CRC diagnosed before the age of 60. The presence of germline alterations in well-known genes related to hereditary CRC syndromes (*APC*, *MUTYH*, and the DNA MMR genes) had been previously ruled out for all probands. The tumors developed by the probands were microsatellite stable, negative for *MLH1* promoter methylation, and showed normal expression of the MMR proteins *MLH1*, *MSH2*, *MSH6*, and *PMS2*. The entire cohort was previously described in detail.<sup>15-17</sup>

For replication purposes, an independent hereditary non-polyposis CRC cohort was available, and comprised 473 families including 488 MMR-proficient cancer affected patients, 96% of them affected with CRC. The mean age at cancer diagnosis was 49 (range: 16-82). Among the 473 studied families, 58 (12.2%) fulfilled the Amsterdam criteria, 385 (81.4%) the Bethesda guidelines, and the remaining 30 (6.3%) none of the

**Abbreviations used in this paper:** CETSAs, cellular thermal shift assay; CRC, colorectal cancer; DEDID, death effector domain-interacting domain; FAF1, Fas-associated factor 1; FID, Fas-interacting domain; LOH, loss of heterozygosity; NF-kappa-B, nuclear factor-kappa-B; PCR, polymerase chain reaction; pNA, p-nitroanilide; SNP, single nucleotide polymorphism; sgRNA, single guide RNA; TNF, tumor necrosis factor; TRAIL, TNF-related apoptosis-inducing ligand; UAS, ubiquitin-related domain.

 Most current article

© 2020 by the AGA Institute. Published by Elsevier Inc. This is an open access article under the CC BY-NC-ND license (<http://creativecommons.org/licenses/by-nc-nd/4.0/>).

0016-5085

<https://doi.org/10.1053/j.gastro.2020.03.015>

established criteria for hereditary nonpolyposis CRC. Detailed description of the cohort may be found in Belhadj et al.<sup>18</sup>

This study was approved by the institutional ethics committee (IDIBAPS: 2011/6440; IDIBELL: PR247/15) and written informed consent was obtained in all cases.

For details on exome sequencing and variant prioritization in initial cohort, mutation identification in pooled samples in replication cohort, variant validation, segregation analysis, and tumor loss of heterozygosity (LOH), as well as additional pathogenicity prediction tools, see the [Supplementary Material](#).

### Immunohistochemistry

Immunostains were performed on histological 2- $\mu$ m sections from colon tumor and normal mucosa from patient III-5 of family FAM13. More detailed information is provided in the [Supplementary Material](#).

### Functional Characterization of Genetic Variants

**Cell lines.** The DLD-1 human CRC cell line was purchased from the American Type Culture Collection (ATCC, Manassas, VA) and cultured in RPMI-1640 medium supplemented with 10% fetal bovine serum (Gibco, Waltham, MA), at 37°C in 5% CO<sub>2</sub>.

**Plasmids.** LentiCRISPRv2-Puro (#98290; Addgene, Cambridge, MA) and pcDNA3-beta-catenin vectors were available. FAF1 ORF (NM\_007051) cloned into pcDNA3.1+C-(K)-DYK expression vector (OHu13027D, FLAG-tagged) was purchased from GenScript (Nanjing, China).

**Antibodies.** Monoclonal antibody against FAF1 (ab183045) was from Abcam (Cambridge, UK). THE DYKDDDDK antibody (A00187) was from GenScript. Anti-p65 (D14E12), anti-GAPDH (14C10), and anti-beta-catenin (D10A8) were purchased from Cell Signaling (Danvers, MA). Anti-PCNA (sc 9857-R) was from Santa Cruz Biotechnology (Dallas, TX). Goat anti-rabbit (SA5-10036) and anti-mouse (SA5-10176) DyLight 800 secondary antibodies were purchased from Thermo Fisher Scientific (Waltham, MA).

**CRISPR/Cas9-mediated FAF1 knockout generation.** The Benchling (<http://benchling.com>) and the MIT (<http://crispr.mit.edu>) CRISPR tools were used to design the single guide RNA (sgRNA) against the coding region of the FAF1 gene. The sgRNA was cloned into the LentiCRISPRv2-Puro vector and transiently transfected into the DLD-1 CRC cell line. Two days later, transfected cells were puromycin-selected (4  $\mu$ g/mL) and seeded into 96-well plates at a density of 1 cell/well. After 3 weeks, several clones were characterized and selected for further analysis. FAF1 editing was validated by Sanger sequencing, and gene inactivation was checked by quantitative real-time polymerase chain reaction (PCR) and Western blot. The detailed protocol is included in the [Supplementary Material](#).

**Site-directed mutagenesis.** The Q5 Site-Directed Mutagenesis Kit (NEB, Ipswich, MA) was used to introduce missense variants in the wild-type pcDNA3.1-FAF1-DYK expression vector, according to the manufacturer's instructions. Mutagenic primers were designed using the NEBaseChanger tool and obtained from IDT (Coralville, IA). Mutagenesis products were verified by Sanger sequencing. Primer details are in the [Supplementary Table 4](#).

**Protein extraction and Western blot.** To obtain whole-cell protein extracts, cells were lysed with RIPA buffer.

To assess nuclear factor (NF)-kappa-B translocation and beta-catenin accumulation, cytoplasmic and nuclear protein fractions were separated by hypotonic lysis. Equal amounts of protein lysates were resolved in NuPAGE Bis-Tris protein gel electrophoresis and transferred onto PVDF membranes (Millipore, Bedford, MA), according to manufacturer's protocols (Thermo Fisher). Proteins were blotted with the indicated primary and secondary DyLight antibodies and detected by using the Odyssey Imaging System (LI-COR, Lincoln, NE). The detailed protocol is included in the [Supplementary Material](#).

**RNA extraction and quantitative real-time PCR.** Total RNA extraction was performed with the RNeasy Mini Kit according to manufacturer's instructions (Qiagen, Hilden, Germany). RNA retrotranscription and PCR amplification details are included in the [Supplementary Material](#).

**Functional assays.** DLD-1 knockout clones for FAF1 were transiently transfected with wild-type (pWT) or mutated (pArg85Pro, pAsp371Asn) plasmids using X-tremeGENE HP DNA transfection reagent. Two days later, cells were subjected to selection with 1000  $\mu$ g/mL of G418 (InvivoGen, San Diego, CA) for 72 hours, as the FAF1 expression pcDNA3.1 vector carries a neomycin resistance cassette. Neomycin-resistant cells were allowed to recover in complete RPMI medium for 2 additional days before performing functional tests.

### Cellular Thermal Shift Assay (CETSA)

Cells expressing wild-type or missense variants were harvested, washed with phosphate-buffered saline, and equally distributed into PCR tubes. Cell suspensions were shortly heated to 6 different temperatures (from 53°C to 58°C,  $\pm$ 1°C, 3 minutes) and immediately snap-frozen in a dry ice/ethanol bath. Subsequently, cells were lysed by 3 freeze-thaw cycles. After heating, stable proteins remain soluble while unstable proteins denature and precipitate, permitting their isolation by high-speed centrifugation (16,000g, 20 minutes at 4°C). Soluble protein fractions were run on Western blots for the protein melting curve analysis.

### Apoptosis

A colorimetric caspase-3 activity assay was performed according to the manufacturer's instructions, with some modifications (Sigma Aldrich, St Louis, MO). Briefly, cells were stimulated with 20 ng/mL of tumor necrosis factor (TNF)-related apoptosis-inducing ligand (TRAIL) at the indicated time points and lysed in 30  $\mu$ L of lysis buffer. Protein concentrations were determined by using the Pierce BCA Protein Assay Kit (Thermo Fisher) and 50  $\mu$ g of each protein extract was assayed with the colorimetric caspase-3 substrate Ac-DEVD-pNA. The release of the yellow chromophore p-nitroanilide (pNA) was measured in an Epoch Microplate Spectrophotometer (BioTek, Winooski, VT) at 405 nm. Caspase-3 activity was calculated in comparison to a pNA standard curve.

### Wnt Signaling

FAF1 wild-type (FAF1<sup>WT</sup>) and FAF1 knockout (FAF1<sup>KO</sup>) cells were cotransfected with a pcDNA3-beta-catenin expression vector together with the pcDNA3 control empty vector or one of the FAF1 vectors (pWT, pArg85Pro, pAsp371Asn), as previously described. When indicated, after cell selection and recovery, cells were treated with the proteasome inhibitor

MG132 (10 μM) for 4 hours. Transfected cells were harvested to extract the cytoplasmic protein fraction, and beta-catenin was detected by Western blotting.

Cell proliferation, colony formation, and migration methods are detailed in the [Supplementary Material](#).

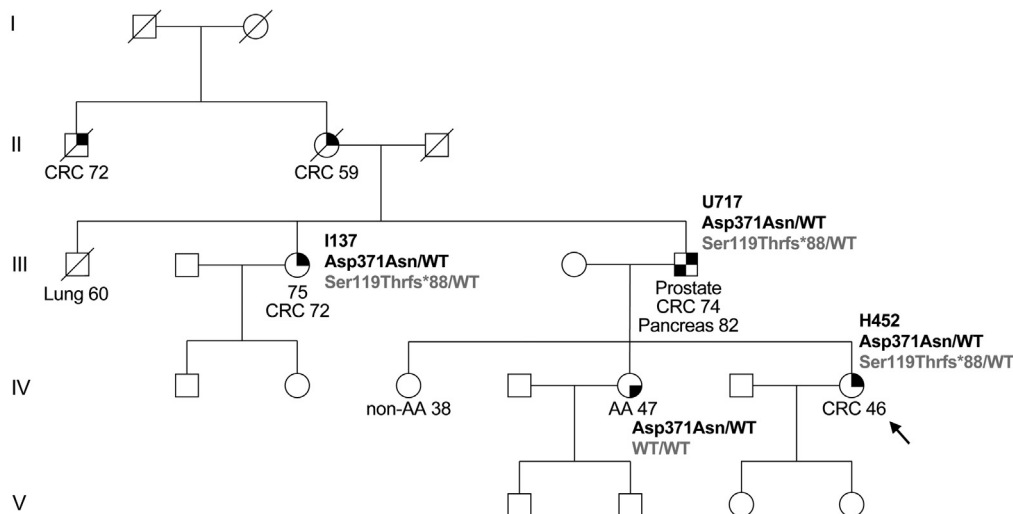
## Results

The variant prioritization strategy applied to whole-exome sequencing data obtained from the initial unaffiliated familial cohort (75 individuals from 40 families) selected a *FAF1* (Fas-associated factor 1) missense variant (c.1111G>A p.Asp371Asn), predicted pathogenic by in silico algorithms. The *FAF1* variant was noticeable among others due to the gene function as a mediator of apoptosis and a negative regulator of both NF-kappa-B and Wnt signaling pathways. The variant was identified in an Amsterdam-positive family of Spanish origin with 5 CRC cases and 3 affected generations (FAM13; [Figure 1](#)). The identified variant was initially detected in 3 CRC-affected family members (ages at diagnosis 46–74) and in 1 relative diagnosed with advanced adenoma at

age 47 ([Supplementary Figure 2A](#)). An *RAD52* truncation variant, c.590\_593dupAACC (p.Ser199Thrfs\*88), was also detected in the 3 CRC-affected family members but not in the relative with the advanced adenoma.<sup>15</sup> The 3 CRC-affected members did not share additional genetic variants with a plausible role in cancer predisposition. Targeted gene sequencing of *FAF1* in 473 additional genetically unexplained CRC families yielded the identification of another predicted pathogenic missense variant, c.254G>C (p.Arg85Pro). It was identified in a Bethesda-positive patient with CRC diagnosed at the age of 55 (F-0681-00; [Figure 1](#) and [Supplementary Figure 2B](#)). Additional samples for variant segregation and tumor sample were not available.

The 2 identified missense variants are rare in large population datasets (ExAC database: allele count 5/121,210 for p.Asp371Asn and 19/121,270 for p.Arg85Pro) and are predicted to be pathogenic by most in silico tools (eg, CADD: 36 for p.Asp371Asn and 23.4 for p.Arg85Pro). The p.Arg85Pro variant is located on the FID domain (Fas-interacting domain) of the protein, and the p.Asp371Asn variant affects both the DEDID domain (death effector domain-interacting

### FAM13



### F-0681-00

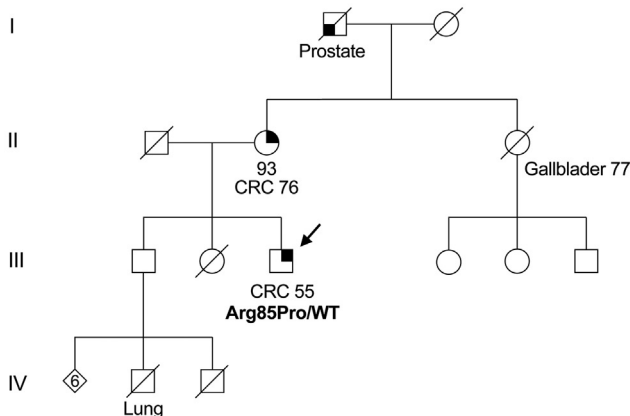


**Figure 1.** Pedigrees of FAM13 and F-0681-00. Filled symbol indicated affected for CRC (upper right quarter) adenoma/s (lower right quarter), prostate and pancreatic cancer (lower left quarter). CRC, lung, prostate, pancreas, and gallbladder refer to the type of cancer. Individual IV-5 from FAM13 presented an advanced adenoma (tubulovillous, high-grade dysplasia, 15 mm) at the age of 47. Cosegregation results for the *FAF1* variant Asp371Asn (black) and *RAD52* Ser199Thrfs\*88 (gray) variants are also shown. AA/non-AA, advanced adenoma/non-advanced adenoma. Ages at diagnosis are indicated. The proband is indicated by an arrow.

domain) and an ubiquitin-related domain (UAS). The p.Arg85Pro variant was predicted to alter the conformational structure of FAF1 (DAMPred), whereas the p.Asp371Asn amino acid change was predicted to impair the acetylation of the nearby K368 residue (MutPred2).

Tumor material from 2 p.Asp371Asn carriers (CRC diagnosed at 46 and 72 years of age, respectively; individuals IV-7 and III-5; Figure 1) was available to evaluate the expression of FAF1 by immunohistochemistry and the presence of LOH. FAF1 protein was expressed both in the cytoplasm and the nucleus of colon tumor cells (Supplementary Figure 1), and LOH was evident, especially in III-5's tumor (Supplementary Figure 3).

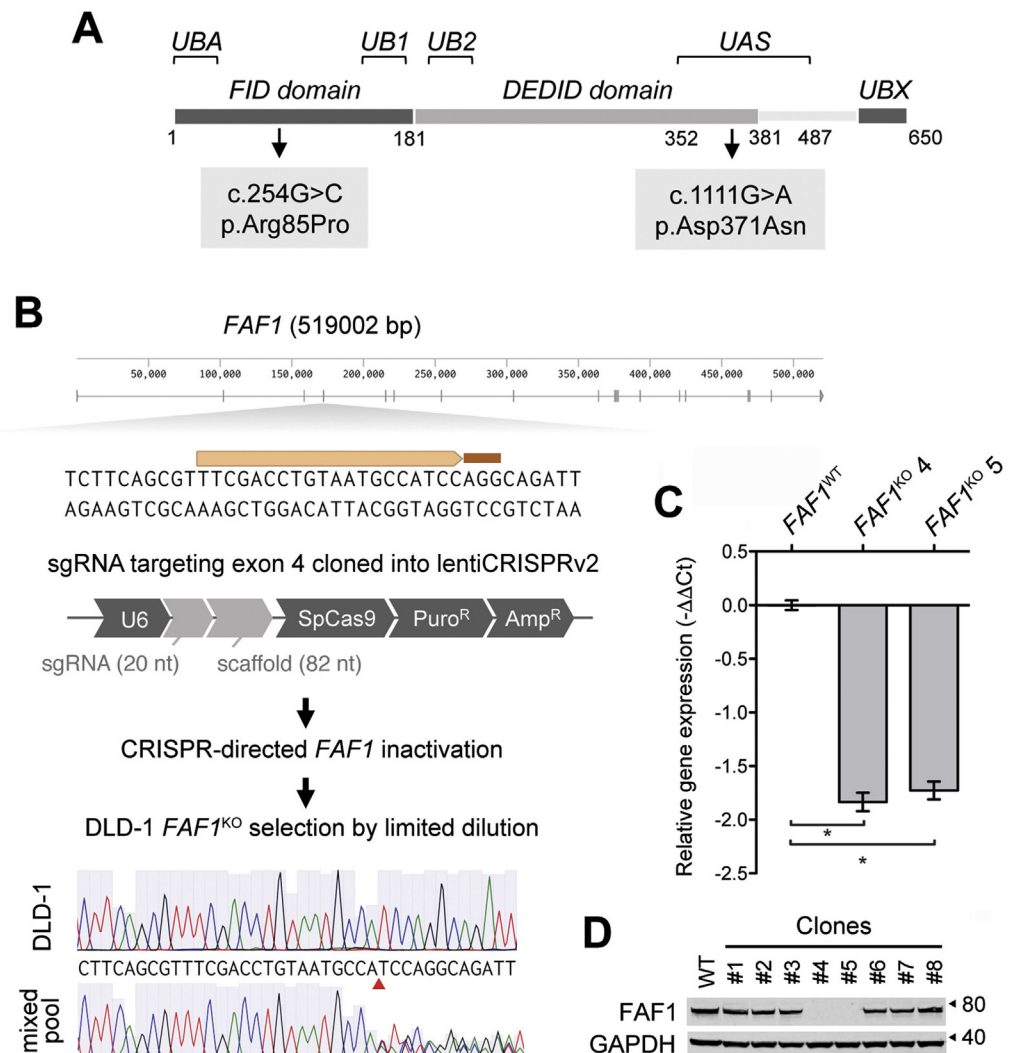
**CRISPR/Cas9 FAF1<sup>KO</sup> Modeling**

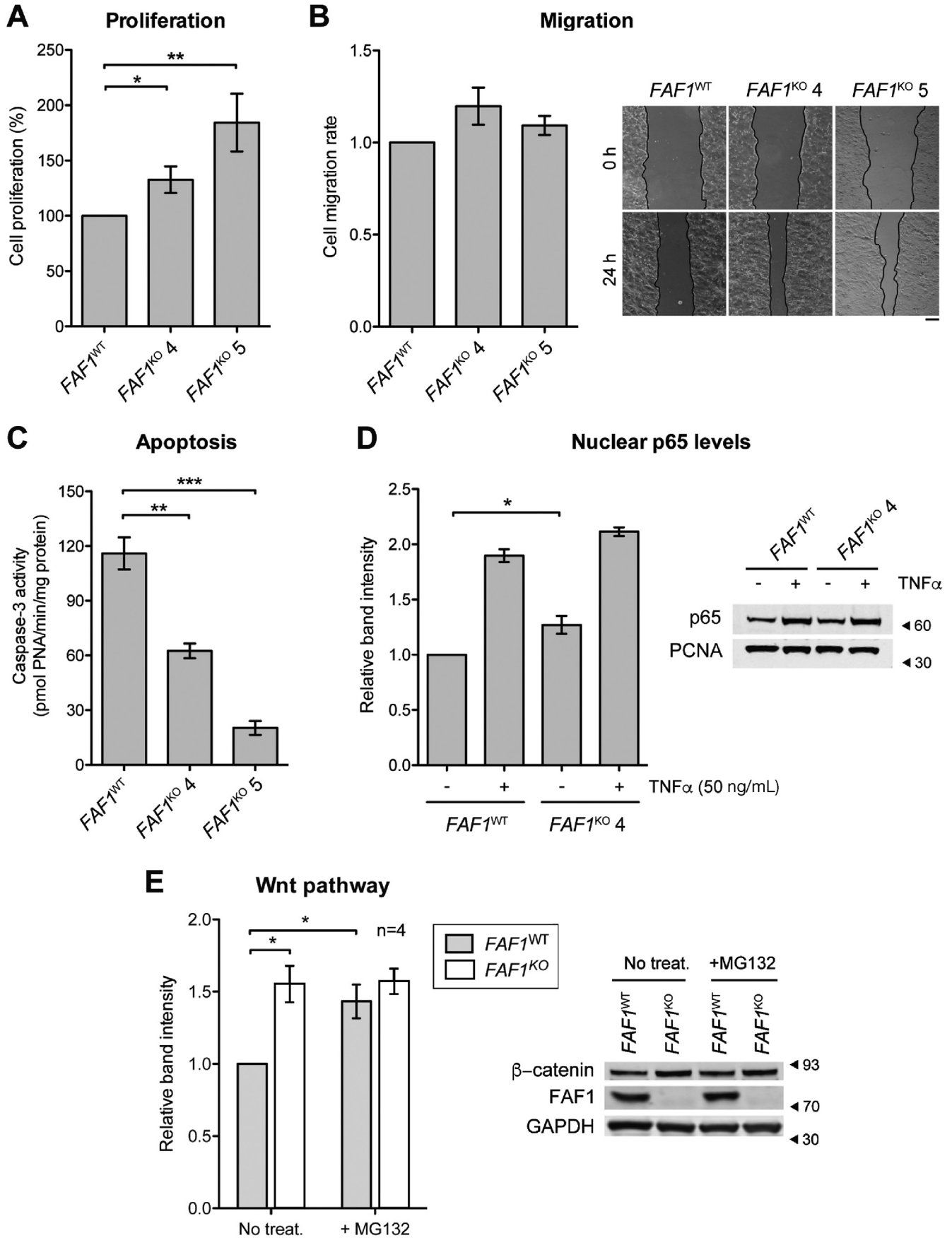
To further validate the suspected role of FAF1 genetic variants on CRC predisposition, we established an FAF1<sup>KO</sup> cellular model by CRISPR/Cas9 gene editing on DLD-1 cells (Figure 2). According to bioinformatic CRISPR prediction tools, an sgRNA targeting the fourth exon was selected because of its favorable on-target and off-target scores. FAF1 gene editing

was checked by Sanger sequencing (Figure 2B), and FAF1 depletion was confirmed by reverse-transcriptase PCR and Western blot (Figure 2C and D). Two FAF1<sup>KO</sup> clones (#4 and #5) were selected for further expansion and characterization.

An initial screening of the tumor suppressor role of FAF1 was performed on CRISPR-generated knockout clones. The functional analysis demonstrated that permanent inactivation of FAF1 resulted in a more malignant phenotype of DLD-1 cells. Knockout clones showed a higher cell proliferation rate on the MTS assay in comparison with FAF1<sup>WT</sup> cells (Figure 3A), as well as a subtle increase in cell migration (Figure 3B). Nevertheless, the most prominent effect was the sustained resistance to programmed cell death of FAF1-depleted cells. After exposing cells to the apoptosis-inducer TRAIL, both caspase-3 activity and cell death were noticeable in FAF1<sup>WT</sup> cells, whereas FAF1<sup>KO</sup> clones showed high resistance to apoptosis (Figure 3C and Supplementary Figure 4). FAF1 has also been described as a negative regulator of the NF-kappa-B signaling pathway, as it prevents the nuclear translocation of p65, a subunit of NF-k-B. Depletion of FAF1 increased both the basal nuclear levels of p65 and the TNF $\alpha$ -induced NF-kappa-B translocation (Figure 3D). Finally,

**Figure 2.** CRISPR/Cas9-mediated FAF1 gene inactivation in the DLD-1 CRC cell line. (A) Mapping of the identified FAF1 missense variants within the functional domains of the protein. (B) Overview of the CRISPR-directed FAF1 inactivation workflow. The 20-nt sgRNA and the 3-nt PAM sequences are depicted. The Sanger sequencing profile of the edited cell pool shows an aberrant sequence signal after the expected break site (red arrow). (C) FAF1 messenger RNA relative expression of the 2 selected FAF1<sup>KO</sup> clones assessed by real-time PCR. Data represent mean  $\pm$  SD (n = 3). (D) Representative Western blot analysis of several FAF1<sup>KO</sup> clones, confirming FAF1 depletion on clones #4 and #5. \*P < .05, analysis of variance with Tukey post hoc test. bp, base pair.





as a ubiquitin-interacting protein, FAF1 has been reported to participate in the regulation of the Wnt signaling pathway. Lower levels of cytoplasmic beta-catenin were detected in *FAF1*<sup>WT</sup> cells in comparison with *FAF1*<sup>KO</sup> cells, confirming the participation of FAF1 in beta-catenin degradation (Figure 3E). Moreover, MG132 treatment promoted the accumulation of beta-catenin in *FAF1*<sup>WT</sup> cells to levels comparable to *FAF1*<sup>KO</sup> cells, indicating its participation in the proteasomal degradation of beta-catenin. These results supported the tumor suppressor role of *FAF1*, which was in line with the hypothesis that mutations affecting its correct functioning could lead to tumor development.

### Functional Characterization of Germline Variants

To evaluate the functional effect of the identified *FAF1* variants, site-directed mutagenesis was performed on a vector carrying the wild-type ORF of *FAF1*. Both c.254G>C and c.1111G>A mutations were PCR-generated and verified by Sanger sequencing (Figure 4A). None of them affected *FAF1* RNA or protein expression (Figure 4B and C). In this line, a time-course expression analysis showed that wild-type and mutated *FAF1* ORFs were equally expressed after transfection (Figure 4D), so the potential pathogenic mechanism of these variants appeared to be unrelated with their expression levels. Still, an amino acid exchange is an event that can disturb the conformational structure of a protein, thus compromising its stability and functionality. Therefore, we performed a CETSA assay to analyze the thermal stability of p.Arg85Pro and p.Asp371Asn variants within the cellular environment. The protein melting curve analysis revealed that both substitutions had reduced FAF1 protein stability in comparison with its wild-type form (Figure 4E). The instability of the p.Asp371Asn variant was already noticeable from lower point temperatures. Altogether, these results suggest that *FAF1* missense alterations might contribute to protein dysfunction.

Because both missense variants seemed to cause protein instability, we proceeded to functionally characterize them by targeting the main cellular and molecular pathways in which *FAF1* participates. As *FAF1* is a component of the Fas-death-inducing signaling complex (Fas-DISC), cell resistance to apoptosis was first analyzed by measuring caspase-3 activation. DLD-1 *FAF1*<sup>KO</sup> clones #4 and #5 were transiently transfected with pWT, pArg85Pro, or pAsp371Asn *FAF1* vectors and exposed to TRAIL stimulation. When we rescued the expression of wild-type *FAF1*, cells were sensitive to TRAIL-induced apoptosis, whereas cells expressing both p.Arg85Pro and p.Asp371Asn *FAF1* variants were more

resistant to cell death (Figure 5A and Supplementary Figure 5).

Another key feature of *FAF1* is the regulation of NF-kappa-B activity by preventing its nuclear translocation. After *FAF1* variant transfection, the subcellular location of the p65 NF- $\kappa$ B subunit was assessed. Cells expressing either p.Arg85Pro or p.Asp371Asn variants subtly accumulated more p65 into the nucleus in comparison with those expressing wild-type *FAF1*. A similar trend was observed for TNF $\alpha$ -stimulated cells, on which the highest amount of nuclear p65 was detected in cells expressing the pAsp371Asn *FAF1* variant (Figure 5B). To further confirm the contribution of *FAF1* missense variants on NF-kappa-B activation, we evaluated the expression of Cyclin D1 (*CCND1*), one of its downstream effector genes. Again, after TNF $\alpha$  treatment, *FAF1* p.Asp371Asn cells exhibited a small increase in *CCND1* expression in comparison with its wild-type counterpart (Figure 5C). Next, as *FAF1* negatively regulates the Wnt signaling pathway, we tested whether *FAF1* missense variants may impair the beta-catenin degradation driven by *FAF1* under basal conditions. Both missense variants promoted an increased beta-catenin accumulation in the cytoplasm, an effect that was especially remarkable on cells expressing the pAsp371Asn *FAF1* variant (Figure 5D). Together, these results support the pro-tumorigenic consequences of FAF1 malfunction on NF-kappa-B and Wnt signaling.

To further explore the functional significance of *FAF1* variants on cell malignancy, additional biological capabilities were assessed, including cell proliferation, colony formation, and cell migration. On transfection, cells expressing both p.Arg85Pro and p.Asp371Asn variants showed higher proliferative rate (Figure 6A) and colony formation capacity (Figure 6B and C) in comparison with the rescued wild-type phenotype. The proliferative effect was quite remarkable on clone *FAF1*<sup>KO</sup> #4 and, at a lower rate, the same trend was observed for clone *FAF1*<sup>KO</sup> #5. Regarding cell migration, the *FAF1*<sup>KO</sup> #4 clone expressing p.Arg85Pro and p.Asp371Asn *FAF1* variants showed an increased wound-healing potential in comparison with cells transfected with the wild-type form of *FAF1* (Figure 6D).

## Discussion

We identified 2 rare genetic variants with plausible pathogenicity in the *FAF1* gene in 2 independent cohorts of unaffiliated familial CRC. A thorough functional characterization of both variants was performed in a CRISPR/Cas9 cellular model to further confirm their pathogenicity and involvement in germline predisposition to CRC, including assays for proliferation, colony formation, cell migration,

**Figure 3.** *FAF1* inactivation enhances a malignant phenotype. (A) MTS cell viability assay on DLD-1 (*FAF1*<sup>WT</sup>) and *FAF1*<sup>KO</sup> clones cultured for 72 hours. (B) Cell migration evaluation by determining the scratched area at the start point and after 24 hours of wound generation. On the right, representative images of the wound closure. Scale bar, 200  $\mu$ m. (C) Apoptosis resistance of both *FAF1*<sup>KO</sup> #4 and #5 clones after 16 hours of TRAIL treatment. (D) Assessment of p65 translocation in *FAF1*<sup>KO</sup> #4 by Western blot analysis of nuclear lysates at basal levels (-TNF $\alpha$ ) or after TNF $\alpha$ -stimulation. (E) beta-catenin detection in cytoplasmic protein lysates of *FAF1*<sup>WT</sup> and *FAF1*<sup>KO</sup> cells. When indicated, cells were treated with MG132. \**P* < .05, \*\**P* < .01, \*\*\**P* < .001, analysis of variance with Tukey post hoc test. Unless otherwise indicated, data represent mean  $\pm$  standard deviation (n = 3).

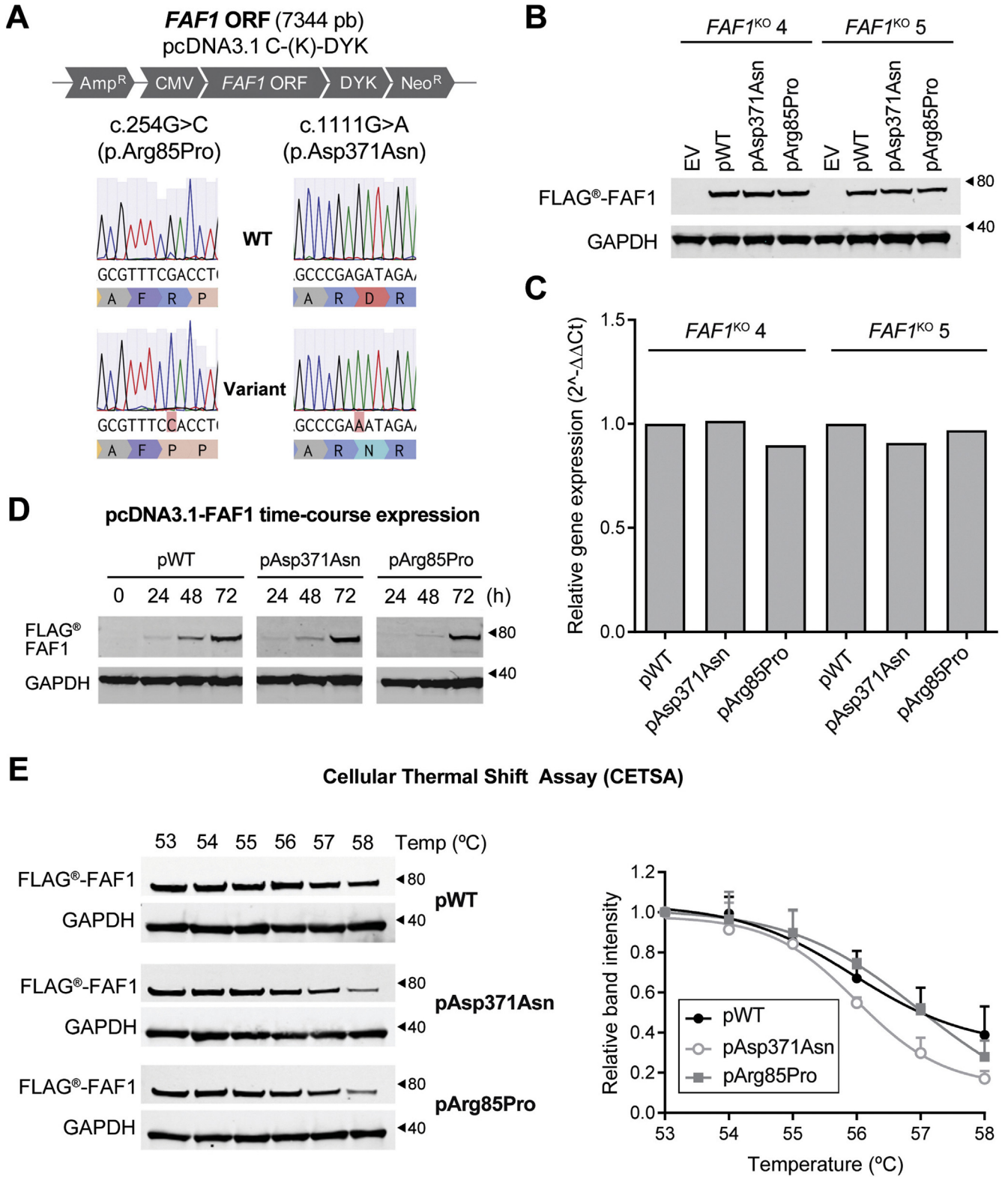


**Figure 4.** Assessment of c.254G>C and c.1111G>A *FAF1* variants expression and protein stability. (A) Site-directed mutagenesis of the pcDNA3.1-*FAF1*-DYK vector. Sanger sequencing verification of the specific nucleotide substitutions (c.254G>C and c.1111G>A) are depicted in red. (B) Western blot analysis and (C) real-time PCR quantification of the expression levels of the indicated FLAG-tagged *FAF1* transfected vectors at both protein and messenger RNA levels, respectively. EV, empty vector. (D) Time-course protein expression analysis on *FAF1*<sup>KO</sup> #4 clone revealing the pcDNA3.1 expression peak 72 hours after transfection. No remarkable expression differences were observed between *FAF1* vectors at the indicated timepoint. (E) Representative Western blot for the CETSA assay of FLAG-tagged *FAF1* transfected cells, either with wild-type or missense variants. On the right, band intensity quantification by densitometry. All data were normalized to the amount of protein detected for each condition at the lowest test temperature and fitted by a 4-parameter logistic (4PL) regression. Data represent mean ± standard deviation (n = 3).



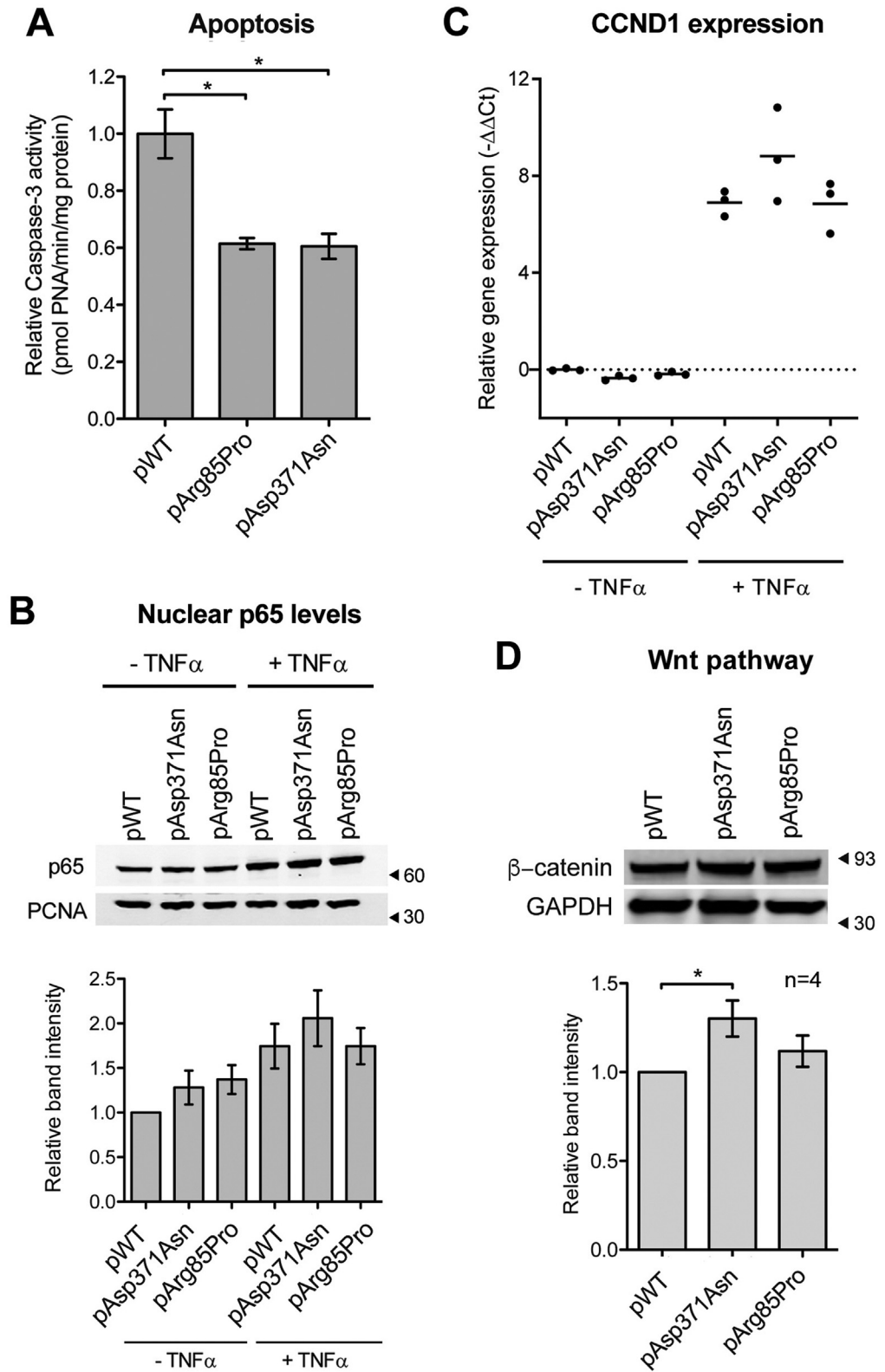
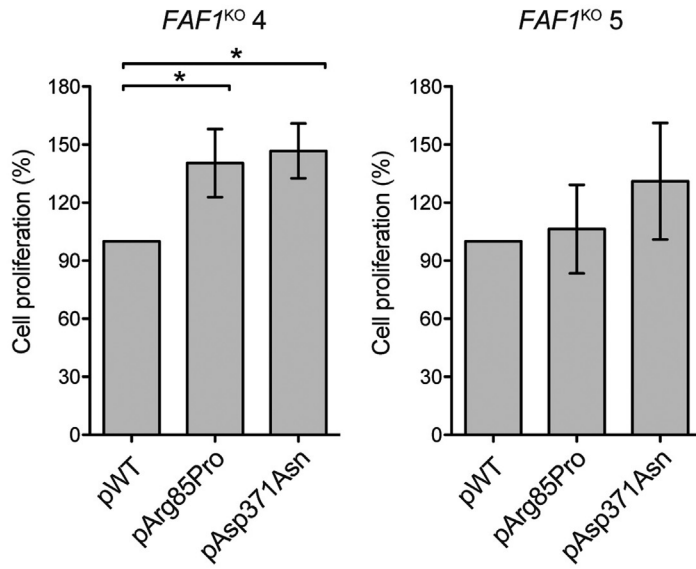
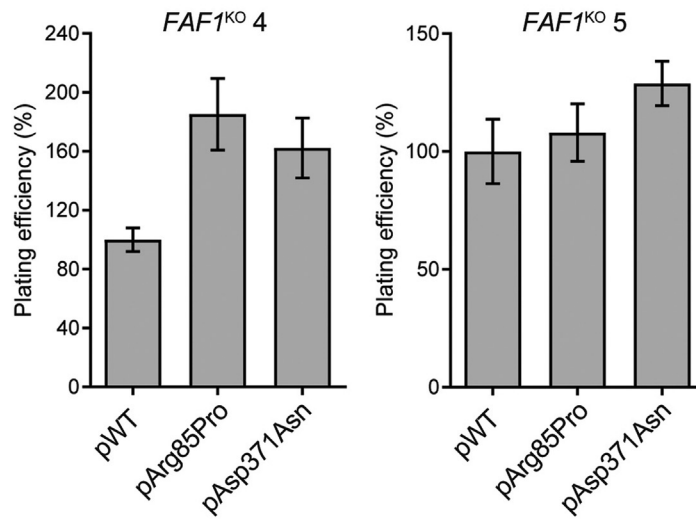


**Figure 5.** *FAF1* variants contribute to apoptosis resistance as well as deregulation of NF-kappa-B and Wnt signaling pathways. *FAF1*<sup>KO</sup> #4 clone was transfected with pWT, pArg85Pro, or pAsp371Asn *FAF1* variants. (A) Determination of caspase-3 activity after TRAIL-induced apoptosis. (B) Western blot analysis of p65 nuclear translocation at basal levels (-TNF $\alpha$ ) or after TNF $\alpha$ -stimulation and (C) real-time PCR quantification of *CCND1* expression levels under the same experimental conditions, assayed in triplicate for *FAF1*<sup>KO</sup> #4. (D) beta-catenin detection in cytoplasmic protein lysates on *FAF1*<sup>KO</sup> cells cotransfected with a pcDNA3 beta-catenin expression vector together with the indicated *FAF1* vectors. Unless otherwise indicated, data on bar graphs represent mean  $\pm$  SD (n = 3). \**P* < .05, analysis of variance with Tukey post hoc test.

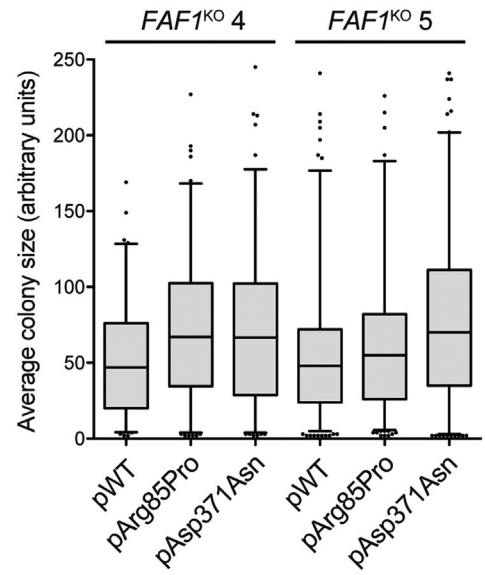
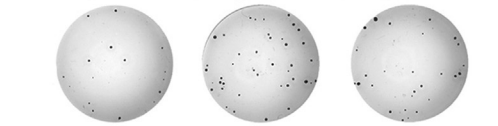
**A Proliferation**



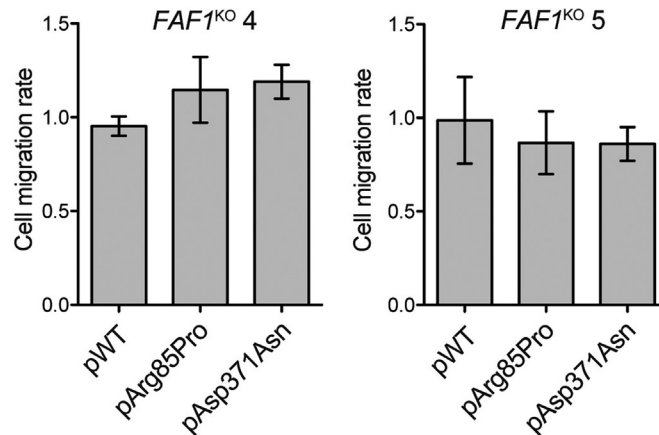
**B Colony formation**



**C**



**D Migration**



BASIC AND TRANSLATIONAL AT

protein stability, resistance to apoptosis, and both NF-kappa-B and Wnt signaling.

The *FAF1* genetic variant was prioritized over an *RAD52* genetic variant in family FAM13 due to additional segregation in an advanced adenoma case. Human *RAD52* can be considered a nonessential gene,<sup>19</sup> whereas *FAF1* is necessary for correct embryonic development.<sup>20</sup> Accordingly, when using the pLI score to estimate their tolerance of loss-of-function variation,<sup>21</sup> *RAD52* pLI score is 0 as compared with 1 for *FAF1*. Overall, these will be suggesting that the latter gene will be more intolerant to mutation and more likely to be involved in cancer predisposition.

*FAF1* is an evolutionary conserved proapoptotic scaffolding protein. It contains 2 apoptosis-related domains (FID and DEDID), as well as several ubiquitination-associated functional domains. It is considered a component of the death-inducing signaling complex (DISC), and it participates in both receptor-dependent<sup>22</sup> and independent<sup>23</sup> apoptosis pathways. Moreover, *FAF1* retains the NF-kappa-B subunit p65 in the cytoplasm via physical interaction, thus inhibiting NF-kappa-B nuclear translocation and activation.<sup>24</sup> In addition, its ubiquitin-binding capacity antagonizes the canonical Wnt signaling pathway<sup>25</sup> and participates in the DNA replication fork dynamics.<sup>26</sup> Therefore, *FAF1* has been contemplated as a tumor suppressor gene, whose downregulation may contribute to tumorigenesis. Our functional characterization of *FAF1*<sup>KO</sup> clones confirmed the involvement of this protein in apoptosis resistance and cell cycle deregulation.

The identified *FAF1* missense mutations in the present study are located in well-defined functional domains. The c.254G>C variant (p.Arg85Pro) is included in the FID domain, whereas the c.1111G>A variant (p.Asp371Asn) is located inside both the helix-rich DEDID and the UAS domains.<sup>27</sup> In silico pathogenicity tools predicted a possible pathogenic conformational change of *FAF1* p.Arg85Pro, as well as a loss of acetylation of the K368 residue in *FAF1* p.Asp371Asn. Acetylation usually works as a stabilizing mechanism, preventing the ubiquitination and subsequent proteasomal degradation of the protein.<sup>28</sup> These results were reinforced by the CETSA assay, which confirmed that both amino acid substitutions altered protein stability, thus potentially modifying protein-protein interactions.

We then assessed whether p.Arg85Pro and p.Asp371Asn variants affected the main cellular processes in which *FAF1* participates. Cells expressing p.Arg85Pro and p.Asp371Asn *FAF1* variants were more resistant to TRAIL-induced apoptosis, which is consistent with the involvement of both FID and DEDID domains in the death signaling cascade. Higher NF-kappa-B activity and cytoplasmic beta-catenin accumulation were detected mainly in p.Asp371Asn *FAF1*

expressing cells, which may be explained by the location of this mutation inside the overlapping domains DEDID and UAS. The DEDID domain is the one that drives the p65-*FAF1* interaction and its retention into the cytoplasm.<sup>24</sup> In the case of beta-catenin, although the specific mechanism by which *FAF1* promotes its degradation is still unknown, it seems to be related to its ubiquitin-binding domains.<sup>25</sup> In this line, Kim et al<sup>29</sup> described that mutations disturbing the highly conserved positive surface patch in the UAS domain of *FAF1* (352-487) conducted to beta-catenin stabilization. Finally, the expression of both mutations increased the proliferation rate of cells and cell survival on colony formation assays. To sum up, our functional characterization results are consistent with a pathogenic role for both identified *FAF1* missense variants.

Our findings are also in agreement with accumulating evidence regarding the tumor suppressor profile of *FAF1* and its involvement in cancer susceptibility. Single nucleotide polymorphism (SNP) testing described the presence of 28 SNPs in the *FAF1* genomic region that may be associated with a high risk of gastric cancer,<sup>30</sup> as well as 22 SNPs in the *FAF1\_CDKN2C* locus that may predispose to an increased risk for papillary thyroid cancer.<sup>31</sup> Because of its tumor suppressor profile, loss or downregulation of somatic *FAF1* could also be expected in human cancer. At the genomic level, losses, deletions, or intragenic breakpoints at the *FAF1* locus have been detected in uterine cervix carcinomas,<sup>32</sup> glioblastoma patients,<sup>33</sup> and mantle cell lymphoma cell lines.<sup>34</sup> In fact, *FAF1* is located in the chromosomal region 1p32.3, recurrently lost in somatic CRC.<sup>35</sup> Furthermore, *FAF1* downregulated expression has been frequently reported in human gastric carcinomas.<sup>36,37</sup>

The balance between survival and programmed cell death is an important homeostatic process that, when disrupted, can facilitate the development of cancer. This equilibrium is specially regulated in normal colonic epithelial cells at the base of crypts, which are highly prone to apoptosis.<sup>38</sup> Therefore, a special role can be hypothesized for those tumor suppressor genes with proapoptotic functions or negatively regulating both Wnt and NF-kappa-B pathways. Accordingly, we can hypothesize that *FAF1*, when disrupted, will deviate the normal homeostatic process and lead to resistance to cell death. In this regard, several studies have already proposed new candidate CRC predisposing genes involved in apoptosis. The pathogenicity of a germline variant in the proapoptotic *UNC5C* gene was validated and suggested to increase the risk for CRC,<sup>39</sup> although with controversy.<sup>40</sup> A screening study of a Finnish cohort identified 2 truncating variants in the *UACA* gene, which was proposed as a novel candidate gene.<sup>41</sup> Similarities can be found between *UACA* and *FAF1*, as both genes promote apoptosis and control the

**Figure 6.** *FAF1* variants also contribute to the malignant cell transformation. *FAF1*<sup>KO</sup> #4 and #5 clones were transfected with pWT, pArg85Pro, or pAsp371Asn *FAF1* variants. (A) MTS cell viability assay after 72 hours of culturing. (B) Plating efficiency of cells (ie, colonies originated from single cells) as well as (C) the growth capacity of cells in the colony formation assay. Representative images of crystal violet staining of clone *FAF1*<sup>KO</sup> #4 are shown. (D) Cell migration evaluation by determining the scratched area at the start point and after 24 hours of wound generation. Data on bar graphs represent mean ± standard deviation (n = 3). \**P* < .05, analysis of variance with Tukey post hoc test.

nuclear factor NF-kappa-B activity. In addition, in a previous study from our research group, we postulated *NFKBIZ* as a novel CRC candidate gene, as it interferes with the DNA binding capacity of both p50 and p65 NF-kappa-B subunits.<sup>15</sup> These biological processes can be relevant not only in CRC predisposition but also in germline susceptibility to other neoplasms. For example, germline mutations in the *FAS* gene, one of the main sensors of the extrinsic apoptosis pathway, are associated with the development of autoimmune lymphoproliferative syndrome and a high risk for both Hodgkin and non-Hodgkin lymphoma.<sup>42,43</sup>

Taking into account the variants found in our series, the *FAF1* frequency in familial CRC could be considered approximately 0.4% (2/513). When adding other genes involved in apoptosis (*UNC5C*, *UACA*, *NFKBIZ*) with reported variants in familial CRC cohorts, the frequency of apoptosis defects could rise to >1%.<sup>39-41,44</sup> Undoubtedly, analysis of additional larger familial CRC cohorts is needed to provide further information about the prevalence and implication of mutations in *FAF1* and other apoptosis-related genes in hereditary CRC.

In summary, our findings suggest germline *FAF1* mutations may be implicated in inherited susceptibility to CRC, and postulate resistance to apoptosis as the plausible underlying mechanism.

## Supplementary Material

Note: To access the supplementary material accompanying this article, visit the online version of *Gastroenterology* at [www.gastrojournal.org](http://www.gastrojournal.org), and at <https://doi.org/10.1053/j.gastro.2020.03.015>.

## References

1. Ferlay J, Colombet M, Soerjomataram I, et al. Estimating the global cancer incidence and mortality in 2018: GLOBOCAN sources and methods. *Int J Cancer* 2018; 144:ijc.31937.
2. Lichtenstein P, Holm NV, Verkasalo PK, et al. Environmental and heritable factors in the causation of cancer—analyses of cohorts of twins from Sweden, Denmark, and Finland. *N Engl J Med* 2000;343:78–85.
3. Frank C, Sundquist J, Yu H, et al. Concordant and discordant familial cancer: familial risks, proportions and population impact. *Int J Cancer* 2017;140:1510–1516.
4. Yurgelun MB, Kulke MH, Fuchs CS, et al. Cancer susceptibility gene mutations in individuals with colorectal cancer. *J Clin Oncol* 2017;35:1086–1095.
5. Valle L. Recent discoveries in the genetics of familial colorectal cancer and polyposis. *Clin Gastroenterol Hepatol* 2017;15:809–819.
6. Adam R, Spier I, Zhao B, et al. Exome sequencing identifies biallelic MSH3 germline mutations as a recessive subtype of colorectal adenomatous polyposis. *Am J Hum Genet* 2016;99:337–351.
7. Nieminen TT, O'Donohue MF, Wu Y, et al. Germline mutation of RPS20, encoding a ribosomal protein, causes predisposition to hereditary nonpolyposis colorectal carcinoma without DNA mismatch repair deficiency. *Gastroenterology* 2014;147:595–598.
8. Olkinuora A, Nieminen TT, Mårtensson E, et al. Biallelic germline nonsense variant of MLH3 underlies polyposis predisposition. *Genet Med* 2019;21:1868–1873.
9. MacArthur DG, Manolio TA, Dimmock DP, et al. Guidelines for investigating causality of sequence variants in human disease. *Nature* 2014;508:469–476.
10. Hahn MM, de Voer RM, Hoogerbrugge N, et al. The genetic heterogeneity of colorectal cancer predisposition—guidelines for gene discovery. *Cell Oncol* 2016;39:491–510.
11. Wei X, Das J, Fragoza R, et al. A massively parallel pipeline to clone DNA variants and examine molecular phenotypes of human disease mutations. *PLoS Genet* 2014;10:e1004819.
12. Coggins NB, Stultz J, O'Geen H, et al. Methods for scarless, selection-free generation of human cells and allele-specific functional analysis of disease-associated SNPs and variants of uncertain significance. *Sci Rep* 2017;7:15044.
13. Matano M, Date S, Shimokawa M, et al. Modeling colorectal cancer using CRISPR-Cas9-mediated engineering of human intestinal organoids. *Nat Med* 2015; 21:256–262.
14. Bonjoch L, Mur P, Arnau-Collell C, et al. Approaches to functionally validate candidate genetic variants involved in colorectal cancer predisposition. *Mol Aspects Med* 2019;69:27–40.
15. Esteban-Jurado C, Vila-Casadesús M, Garre P, et al. Whole-exome sequencing identifies rare pathogenic variants in new predisposition genes for familial colorectal cancer. *Genet Med* 2015;17:131–142.
16. Esteban-Jurado C, Franch-Expósito S, Muñoz J, et al. The Fanconi anemia DNA damage repair pathway in the spotlight for germline predisposition to colorectal cancer. *Eur J Hum Genet* 2016;24:1501–1505.
17. Franch-Expósito S, Esteban-Jurado C, Garre P, et al. Rare germline copy number variants in colorectal cancer predisposition characterized by exome sequencing analysis. *J Genet Genomics* 2018;45:41–45.
18. Belhadj S, Mur P, Navarro M, et al. Delineating the phenotypic spectrum of the NTHL1-associated polyposis. *Clin Gastroenterol Hepatol* 2017;15:461–462.
19. Rijkers T, Van Den Ouweland J, Morolli B, et al. Targeted inactivation of mouse RAD52 reduces homologous recombination but not resistance to ionizing radiation. *Mol Cell Biol* 1998;18:6423–6429.
20. Adham IM, Khulan J, Held T, et al. Fas-associated factor (FAF1) is required for the early cleavage-stages of mouse embryo. *Mol Hum Reprod* 2008;14:207–213.
21. Lek M, Karczewski KJ, Minikel EV, et al. Analysis of protein-coding genetic variation in 60,706 humans. *Nature* 2016;536:285–291.
22. Ryu S-W, Lee S-J, Park M-Y, et al. Fas-associated factor 1, FAF1, is a member of Fas death-inducing signaling complex. *J Biol Chem* 2003;278:24003–24010.
23. Park M-Y, Ryu S-W, Kim KD, et al. Fas-associated factor-1 mediates chemotherapeutic-induced apoptosis

- via death effector filament formation. *Int J Cancer* 2005; 115:412–418.
24. Park M-Y, Jang HD, Lee SY, et al. Fas-associated Factor-1 inhibits nuclear factor- $\kappa$ B (NF- $\kappa$ B) activity by interfering with nuclear translocation of the RelA (p65) subunit of NF- $\kappa$ B. *J Biol Chem* 2004;279:2544–2549.
  25. Zhang L, Zhou F, van Laar T, et al. Fas-associated factor 1 antagonizes Wnt signaling by promoting  $\beta$ -catenin degradation. *Mol Biol Cell* 2011;22:1617–1624.
  26. Franz A, Pirson PA, Pilger D, et al. Chromatin-associated degradation is defined by UBXN-3/FAF1 to safeguard DNA replication fork progression. *Nat Commun* 2016; 7:10612.
  27. Menges CW, Altomare DA, Testa JR. FAS-associated factor 1 (FAF1): diverse functions and implications for oncogenesis. *Cell Cycle* 2009;8:2528–2534.
  28. Caron C, Boyault C, Khochbin S. Regulatory cross-talk between lysine acetylation and ubiquitination: role in the control of protein stability. *Bioessays* 2005;27:408–415.
  29. Kim H, Rodriguez-Navas C, Kollipara RK, et al. Unsaturated fatty acids stimulate tumor growth through stabilization of  $\beta$ -catenin. *Cell Rep* 2015; 13:495–503.
  30. Hyland PL, Lin S-W, Hu N, et al. Genetic variants in fas signaling pathway genes and risk of gastric cancer. *Int J Cancer* 2014;134:822–831.
  31. Neta G, Brenner AV, Sturgis EM, et al. Common genetic variants related to genomic integrity and risk of papillary thyroid cancer. *Carcinogenesis* 2011;32:1231–1237.
  32. Hidalgo A, Baudis M, Petersen I, et al. Microarray comparative genomic hybridization detection of chromosomal imbalances in uterine cervix carcinoma. *BMC Cancer* 2005;5:77.
  33. Zheng S, Fu J, Vegesna R, et al. A survey of intragenic breakpoints in glioblastoma identifies a distinct subset associated with poor survival. *Genes Dev* 2013;27:1462–1472.
  34. Beà S, Salaverria I, Armengol L, et al. Uniparental disomies, homozygous deletions, amplifications, and target genes in mantle cell lymphoma revealed by integrative high-resolution whole-genome profiling. *Blood* 2009; 113:3059–3069.
  35. Cancer Genome Atlas Network. Comprehensive molecular characterization of human colon and rectal cancer. *Nature* 2012;487:330–337.
  36. Bjørling-Poulsen M, Seitz G, Guerra B, et al. The proapoptotic FAS-associated factor 1 is specifically reduced in human gastric carcinomas. *Int J Oncol* 2003; 23:1015–1023.
  37. Liu AQ, Ge LY, Ye XQ, et al. Reduced FAF1 expression and *Helicobacter* infection: correlations with clinicopathological features in gastric cancer. *Gastroenterol Res Pract* 2012;2012:153219.
  38. Watson AJM. Apoptosis and colorectal cancer. *Gut* 2004;53:1701–1709.
  39. Coissieux MM, Tomsic J, Castets M, et al. Variants in the netrin-1 receptor UNC5C prevent apoptosis and increase risk of familial colorectal cancer. *Gastroenterology* 2011;141:2039–2046.
  40. Mur P, Sánchez-Cuartielles E, Aussó S, et al. Scarce evidence of the causal role of germline mutations in UNC5C in hereditary colorectal cancer and polyposis. *Sci Rep* 2016;6:20697.
  41. Gylfe AE, Katainen R, Kondelin J, et al. Eleven candidate susceptibility genes for common familial colorectal cancer. *PLoS Genet* 2013;9:e1003876.
  42. Poppema S, Maggio E, van den Berg A. Development of lymphoma in Autoimmune Lymphoproliferative Syndrome (ALPS) and its relationship to Fas gene mutations. *Leuk Lymphoma* 2004;45:423–431.
  43. Rahman N. Realizing the promise of cancer predisposition genes. *Nature* 2014;505:302–308.
  44. Kúry S, Garrec C, Airaud F, et al. Evaluation of the colorectal cancer risk conferred by rare UNC5C alleles. *World J Gastroenterol* 2014;20:204–213.

---

Author names in bold designate shared co-first authorship.

Received August 30, 2019. Accepted March 8, 2020.

#### Correspondence

Address correspondence to: Sergi Castellví-Bel, PhD, Institut d'Investigacions Biomèdiques August Pi i Sunyer (IDIBAPS), Rosselló 153, 08036 Barcelona, Spain. e-mail: sbel@clinic.cat.

#### CRediT Authorship Contributions

Laia Bonjoch, PhD (Conceptualization: Lead; Data curation: Lead; Formal analysis: Lead; Investigation: Lead; Methodology: Lead; Software: Lead; Validation: Lead; Visualization: Lead; Writing – original draft: Supporting; Writing – review & editing: Supporting). Sebastià Franch-Expósito, PhD (Conceptualization: Lead; Data curation: Supporting; Formal analysis: Supporting; Investigation: Supporting; Methodology: Supporting; Software: Supporting; Validation: Supporting; Visualization: Supporting; Writing – review & editing: Supporting). Pilar Garre, PhD (Data curation: Supporting; Investigation: Supporting; Methodology: Supporting; Resources: Supporting; Writing – review & editing: Supporting). Sami Belhadj, MSc (Data curation: Supporting; Formal analysis: Supporting; Investigation: Supporting; Methodology: Supporting; Resources: Supporting; Validation: Supporting; Visualization: Supporting; Writing – review & editing: Supporting). Jenifer Muñoz, BSc (Data curation: Supporting; Investigation: Supporting; Methodology: Supporting; Validation: Supporting; Visualization: Supporting; Writing – review & editing: Supporting). Coral Arnau-Collell, MSc (Investigation: Supporting; Methodology: Supporting; Validation: Supporting; Visualization: Supporting; Writing – review & editing: Supporting). Marcos Diaz-Gay, MSc (Formal analysis: Supporting; Investigation: Supporting; Methodology: Supporting; Software: Supporting; Validation: Supporting; Visualization: Supporting; Writing – review & editing: Supporting). Anna Gratacós-Mulleras, MSc (Data curation: Supporting; Formal analysis: Supporting; Investigation: Supporting; Methodology: Supporting; Validation: Supporting; Visualization: Supporting; Writing – review & editing: Supporting). Giulia Raimondi, MSc (Investigation: Supporting; Methodology: Supporting; Resources: Supporting; Writing – review & editing: Supporting). Clara Esteban-Jurado, PhD (Data curation: Supporting; Formal analysis: Supporting; Investigation: Supporting; Writing – review & editing: Supporting). Yasmin Soares de Lima, MSc (Investigation: Supporting; Methodology: Supporting; Validation: Supporting; Visualization: Supporting; Writing – review & editing: Supporting). Cristina Herrera-Pariente, MSc (Investigation: Supporting; Methodology: Supporting; Validation: Supporting; Visualization: Supporting; Writing – review & editing: Supporting). Miriam Cuatrecasas, MD PhD (Investigation: Supporting; Methodology: Supporting; Resources: Supporting; Validation: Supporting; Visualization: Supporting; Writing – review & editing: Supporting). Teresa Ocaña, BSc (Data curation: Supporting; Investigation: Supporting; Resources: Supporting; Writing – review & editing: Supporting). Antoni Castells, MD PhD (Funding acquisition: Supporting; Investigation: Supporting; Resources: Supporting; Writing – review & editing: Supporting). Cristina Fillat, PhD (Investigation: Supporting; Methodology: Supporting; Resources: Supporting; Supervision: Supporting; Writing – review & editing: Supporting). Gabriel Capellá, MD PhD (Funding acquisition: Supporting; Investigation: Supporting; Resources: Supporting; Writing – review & editing: Supporting). Francesc Balaguer, MD PhD (Funding acquisition: Supporting; Investigation: Supporting; Resources: Supporting; Writing – review & editing: Supporting). Trinidad Caldés, PhD (Data curation: Supporting; Funding acquisition: Supporting; Investigation: Supporting; Resources: Supporting; Writing – review & editing: Supporting).

Laura Valle, PhD (Data curation: Supporting; Formal analysis: Supporting; Funding acquisition: Supporting; Investigation: Supporting; Methodology: Supporting; Project administration: Supporting; Resources: Supporting; Supervision: Supporting; Validation: Supporting; Visualization: Supporting; Writing – review & editing: Supporting). Sergi Castellví-Bel, Ph.D. (Conceptualization: Lead; Data curation: Lead; Formal analysis: Lead; Funding acquisition: Lead; Investigation: Lead; Methodology: Supporting; Project administration: Lead; Resources: Lead; Software: Supporting; Supervision: Lead; Validation: Lead; Visualization: Lead; Writing – original draft: Lead; Writing – review & editing: Lead).

#### Conflict of interest

The authors disclose no conflicts.

#### Funding

Laia Bonjoch was supported by a Juan de la Cierva postdoctoral contract (FJCI-2017-32593). Sebastià Franch-Expósito, Coral Arnau-Collell, Jenifer Muñoz, and Cristina Herrera-Pariente were supported by a contract from

CIBEREHD. Marcos Díaz-Gay was supported by a contract from Agència de Gestió d'Ajuts Universitaris i de Recerca -AGAUR- (Generalitat de Catalunya, 2019FI\_B2\_00203) and Yasmin Soares de Lima was awarded an INPhINIT fellowship (LCF/BQ/DI18/11660058) from “la Caixa” Foundation (ID 100010434 funded by the EU Horizon 2020 Programme Marie Skłodowska-Curie grant agreement no. 713673). CIBEREHD, CIBERER, and CIBERONC are funded by the Instituto de Salud Carlos III. This research was supported by grants from Fondo de Investigación Sanitaria/FEDER (16/01292, 17/00878), Fundación Científica de la Asociación Española contra el Cáncer (GCB13131592CAST), Spanish Ministry of Science, Innovation and Universities, co-funded by FEDER funds (SAF2016-80888-R, BIO2017-89754-C2-2R), PERIS (SLT002/16/00398, SLT002/16/0037, Generalitat de Catalunya), CERCA Program (Generalitat de Catalunya), and Agència de Gestió d'Ajuts Universitaris i de Recerca (Generalitat de Catalunya, GRPRE 2017SGR21, GRC 2017SGR653, 2017SGR723, 2017SGR861, 2017SGR1282). This article is based on work from COST Action CA17118, supported by COST (European Cooperation in Science and Technology). [www.cost.eu](http://www.cost.eu).

## Supplementary Material. Exome Sequencing and Variant Identification

### Exome Sequencing and Variant Prioritization in Initial Cohort

Germline DNA samples used for exome sequencing were isolated from peripheral blood using the QIAamp DNA Blood (Qiagen, Hilden, Germany) following the manufacturer's instructions.

Whole-exome sequencing (WES) was performed in samples of selected patients using the HiSeq2000 platform (Illumina, San Diego, CA) and SureSelectXT Human All Exon v5 kit (Agilent, Santa Clara, CA) for exon enrichment. WES cannot reliably detect copy-number variants as in large deletions/duplication/insertions. Indexed libraries were pooled and massively parallel sequenced using a paired-end 2 × 75-base pair read length protocol. Quality control of sequencing data was made in all samples previously to their analysis using the Real-Time Analysis software sequence pipeline (Illumina, San Diego, CA). Burrows-Wheeler Aligner (BWA-MEM algorithm) was used for read mapping to the human reference genome (build hs37d5, based on NCBI GRCh37).<sup>1</sup> PCR duplicates were discarded using MarkDuplicates tool from Picard and then indel realignment and base quality score recalibration were performed with the Genome Analysis Toolkit (GATK).<sup>2</sup>

The GATK tools HaplotypeCaller and MuTect2 were used for SNV and short indels calling for germline and tumor samples, respectively.<sup>2</sup> Regarding variant annotation, different databases were considered, including SnpEff, ANNOVAR, and dbNSFP, for pathogenicity and variant position annotation. PhyloP (phyloP46way\_placental score  $\geq 1.6$ ), SIFT (prediction of damaging), PolyPhen2 (HumVar prediction of probably damaging or possibly damaging), MutationTaster (prediction of disease-causing or disease-causing-automatic), LRT (prediction of deleterious), and CADD (Phred score  $\geq 15$ ) were used for pathogenicity prediction of missense variants. Germline WES data were analyzed through an in-house R language pipeline described in previous studies.<sup>3-5</sup> Functions related with CRC or cancer were prioritized. DNA repair, apoptosis, autophagy, cell growth, cell proliferation, inflammatory response, cell cycle, angiogenesis, cell differentiation, cell adhesion, and chromatin modification, among others, were included.

### Variant Identification in Pooled Samples in Replication Cohort

Patients were screened for genetic variants in *FAF1* using a combination of PCR amplification in pooled DNAs and targeted massively parallel sequencing, as previously described.<sup>6</sup> Primers are listed in [Supplementary Table 2](#). Again, variant prioritization was performed as previously described.<sup>3-5</sup>

### Variant Validation, Segregation Analysis, and Tumor LOH

Results for the prioritized variants in initial and replication cohorts were validated by using specific primers for PCR amplification designed using Primer3Plus<sup>7</sup> and Sanger sequencing (GATC Biotech, Cologne, Germany). Segregation analysis of the prioritized variants was performed when possible in additional family members affected with CRC or advanced adenoma ([Supplementary Figure 2](#)). LOH was tested by comparing Sanger sequencing results including the identified variant from germline and tumor DNA of the same individual. Primers are listed in [Supplementary Table 1](#).

### Additional Pathogenicity Prediction Tools

Besides the bioinformatic pathogenicity tools used in the variant prioritization process, 2 additional in silico tools were used to predict protein structural alterations (DAMPred, <https://zhanglab.ccmb.med.umich.edu/DAMPred/>)<sup>8</sup> and molecular mechanisms that could become altered and lead to protein misfunction (MutPred2, <http://mutpred.mutdb.org/>).<sup>9</sup>

### Immunohistochemistry

Immunostains were performed on histological 2- $\mu$ m sections from colon tumor and normal mucosa from patient III-5 of family FAM13. After deparaffination, antigen retrieval was performed with citrate buffer 10 mM, and tissue was permeabilized with 1% Triton X-100. Peroxidase activity was blocked with 3% hydrogen peroxide. Sections were treated for 2 hours with Dako serum-free protein blocker (Agilent, Santa Clara, CA), incubated for 16 hours with monoclonal rabbit anti-FAF1 antibody at 1/700 dilution (ab183045, Abcam, Cambridge, UK), and for 1 hour with goat anti-rabbit secondary antibody at 37°C (Dako REAL EnVision HRP Rabbit; Agilent). Sections were revealed with diaminobenzidine for 25 seconds (Agilent), counterstained with hematoxylin, and mounted. An Olympus BX41 microscope (Olympus, Tokyo, Japan) was used to visualize the immunostains.

## Functional Characterization of Genetic Variants

### CRISPR/Cas9-mediated *FAF1* Knockout Generation

The Benchling (<http://benchling.com>) and the MIT (<http://crispr.mit.edu>) CRISPR tools were used to design the sgRNA against the coding region of the *FAF1* gene. The top and bottom strands of the sgRNA were purchased from IDT (Coralville, IA) and cloned into the Lenti-CRISPRv2-Puro vector (which also packages the Cas9 coding sequence) as follows. Briefly, LentiCRISPRv2-Puro vector was digested with Esp3I (Thermo Fisher,

Waltham, MA) and run on 0.8% agarose gel. The 12-kb band corresponding to the plasmid backbone was extracted with the QIAquick Gel Extraction Kit (Qiagen, Hilden, Germany). The sgRNA-encoding oligonucleotides were annealed, phosphorylated with the T4 Polynucleotide Kinase (NEB, Ipswich, MA), and ligated into the LentiCRISPR backbone with T4 ligase (NEB, Ipswich, MA). The vector was transiently transfected into the DLD-1 CRC cell line using X-tremeGENE HP DNA transfection reagent (Roche, Basel, Switzerland), thus avoiding the stable expression of Cas9 and reducing its subsequent undesired effects, such as off-target activity and cytotoxicity. Two days later, transfected cells were puromycin-selected (4  $\mu\text{g}/\text{mL}$ ) and CRISPR-editing efficacy on the targeted locus was verified by Sanger sequencing and TIDE webtool analysis.<sup>10</sup> For single-cell cloning, puromycin-resistant cells were seeded into a 96-well plate at a density of 1 cell/well. After 3 weeks, several clones were characterized and selected for further analysis. *FAF1* editing was validated by Sanger sequencing, and gene inactivation was checked by quantitative real-time PCR and Western blot. Primers are listed in [Supplementary Table 3](#).

### Protein Extraction and Western Blot

To obtain whole-cell protein extracts, cells were detached from cell culture plates with Accutase (Sigma Aldrich, St Louis, MO) and lysed with RIPA buffer supplemented with cOmplete Protease Inhibitor Cocktail and PhosSTOP (Roche). To assess NF-kappa-B translocation and beta-catenin accumulation, cytoplasmic and nuclear protein fractions were separated as follows. Cells were resuspended in ice-cold hypotonic buffer (Tris 10 mM, NaCl 10 mM, MgCl<sub>2</sub> 10 mM) and lysed with 1% NP-40. Cytoplasmic proteins were separated from nuclei by high-speed centrifugation, and the nuclear protein fraction was lysed by pulse sonication and RIPA extraction. Sample protein concentrations were determined by using the Pierce BCA Protein Assay Kit (Thermo Fisher, Waltham, MA). Equal amounts of protein lysates were resolved in NuPAGE Bis-Tris protein gel electrophoresis, followed by protein transfer onto Immobilon PVDF membranes (Millipore, Bedford, MA), according to manufacturer's protocols (Thermo Fisher). Proteins were blotted with the indicated primary and secondary Dylight antibodies and detected by using the Odyssey Imaging System (LI-COR, Lincoln, NE).

### RNA Extraction and Quantitative Real-Time PCR

Total RNA extraction was performed with the RNeasy Mini Kit according to manufacturer's instructions (Qiagen). RNA was retrotranscribed using the Applied Biosystems High-Capacity cDNA Reverse Transcription Kit (Thermo Fisher). Multiplex quantitative PCR was performed with the Applied Biosystems (Foster City, CA) 7300 PCR System by using specific TaqMan assays for *FAF1*-FAM (hs00169544\_m1) and *CCND1*-FAM (hs00765553\_m1). The endogenous control gene was *GAPDH*-VIC (4326317E). Relative expression levels of each target gene were calculated for each sample as  $-\Delta\text{Ct}$  values ( $-\Delta\text{Ct} = -[\text{Ct target gene} - \text{Ct endogenous control}]$ ).

### Cell Proliferation

The proliferative capacity of cells was determined using the colorimetric CellTiter 96 Aqueous One Solution Cell Proliferation Assay kit (Promega, Madison, WI). Transfected cells were seeded at a density of 5000 cells per well in a 96-well plate, in quintuplicate. After 72 hours, 20  $\mu\text{L}$  of CellTiter 96 aqueous reagent was added to each well. Plates were incubated at 37°C for 3 hours and absorbance was read at 490 nm using an Epoch Microplate Spectrophotometer (BioTek, Winooski, VT).

### Colony Formation Assay

Single-cell suspensions were prepared with Accutase and by filtration through a 40  $\mu\text{m}$  cell strainer when needed. A total of 200 cells per well were seeded into a 6-well plate in complete growth medium. After 14 days, colonies were fixed in methanol and stained with 0.5% crystal violet (Sigma Aldrich). Colonies were imaged on an EliSpot Reader System (AID GmbH, Strassberg, Germany) and analyzed by ImageJ (National Institutes of Health, Bethesda, MD).

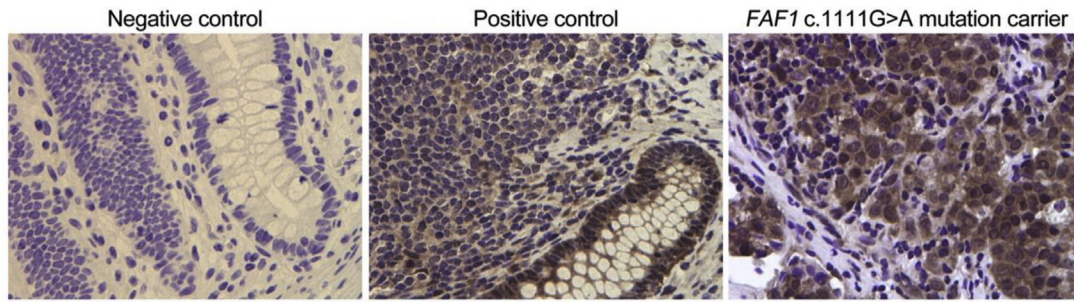
### Migration Assay

The wound-healing assay was performed by seeding transfected cells until confluence in 12-well plates. Cells were treated with 0.2  $\mu\text{g}/\text{mL}$  of mitomycin C to arrest proliferation before scratching the confluent cell monolayer with a sterile pipette tip. Migration was monitored every 24 hours until scratch closure. Images were acquired by using the Cell-R software on an Olympus IX51 microscope (Tokyo, Japan). ImageJ software was used to quantify the scratch closure area at each time point.



## References

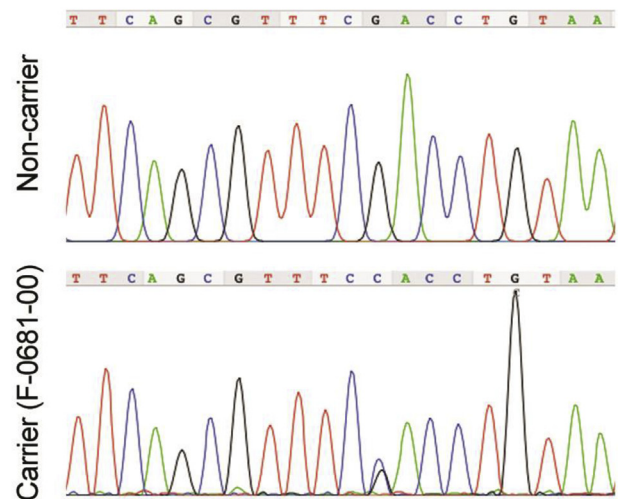
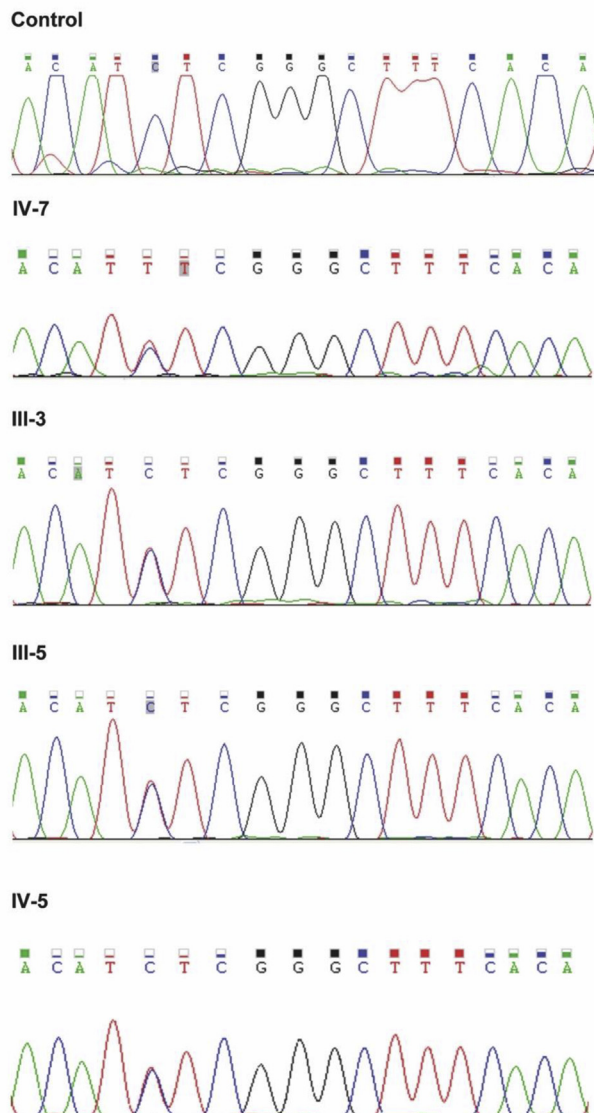
1. Li H, Durbin R. Fast and accurate short read alignment with Burrows-Wheeler transform. *Bioinformatics* 2009;25:1754–1760.
2. McKenna A, Hanna M, Banks E, et al. The Genome Analysis Toolkit: a MapReduce framework for analyzing next-generation DNA sequencing data. *Genome Res* 2010;20:1297–1303.
3. Esteban-Jurado C, Vila-Casadesús M, Garre P, et al. Whole-exome sequencing identifies rare pathogenic variants in new predisposition genes for familial colorectal cancer. *Genet Med* 2015;17:131–142.
4. Esteban-Jurado C, Franch-Expósito S, Muñoz J, et al. The Fanconi anemia DNA damage repair pathway in the spotlight for germline predisposition to colorectal cancer. *Eur J Hum Genet* 2016;24:1501–1505.
5. Franch-Expósito S, Esteban-Jurado C, Garre P, et al. Rare germline copy number variants in colorectal cancer predisposition characterized by exome sequencing analysis. *J Genet Genomics* 2018;45:41–45.
6. Bellido F, Sowada N, Mur P, et al. Association between germline mutations in BRF1, a subunit of the RNA Polymerase III Transcription Complex, and hereditary colorectal cancer. *Gastroenterology* 2018;154:181–194.e20.
7. Untergasser A, Nijveen H, Rao X, et al. Primer3Plus, an enhanced web interface to Primer3. *Nucleic Acids Res* 2007;35(Web Server issue):W71–W74.
8. Quan L, Wu H, Lyu Q, et al. DAMpred: recognizing disease-associated nsSNPs through Bayes-guided neural-network model built on low-resolution structure prediction of proteins and protein-protein interactions. *Mol Biol* 2019;431:2449–2459.
9. Pejaver V, Urresti J, Lugo-Martinez J, et al. MutPred2: inferring the molecular and phenotypic impact of amino acid variants. *bioRxiv* 134981; doi: <https://doi.org/10.1101/134981>.
10. Brinkman EK, Chen T, Amendola M, et al. Easy quantitative assessment of genome editing by sequence trace decomposition. *Nucleic Acids Res* 2014;42:e168.



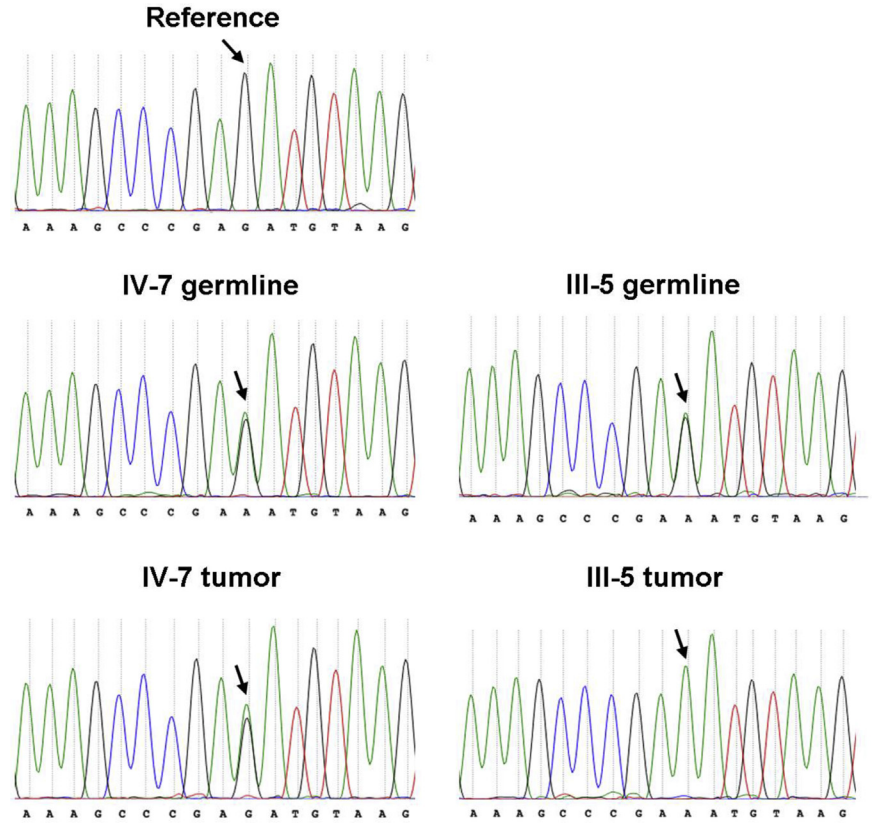
**Supplementary Figure 1.** Immunohistochemistry analysis. FAF1 immunohistochemical staining in normal colonic mucosa of a control individual and tumor tissue of a *FAF1* c.1111G>A mutation carrier (FAM13, individual III-5). A general FAF1 intracellular staining is detected.

(A) c.1111G>A (p.Asp371Asn) *FAF1* variant in FAM13.

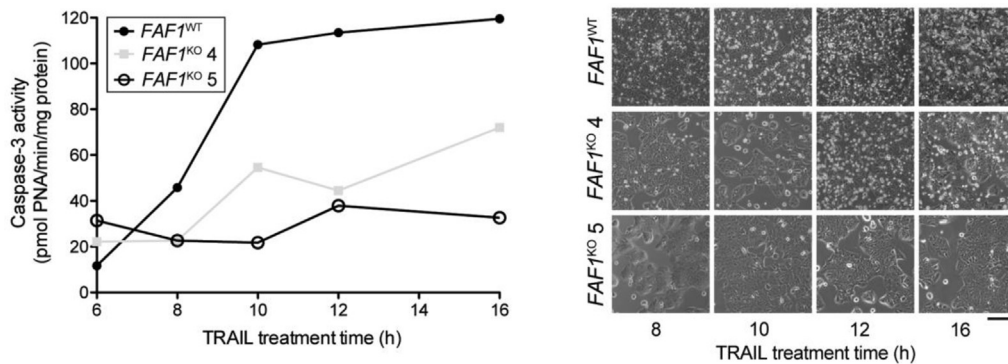
(B) c.254G>C (p.Arg85Pro) *FAF1* variant in F-0681-00.



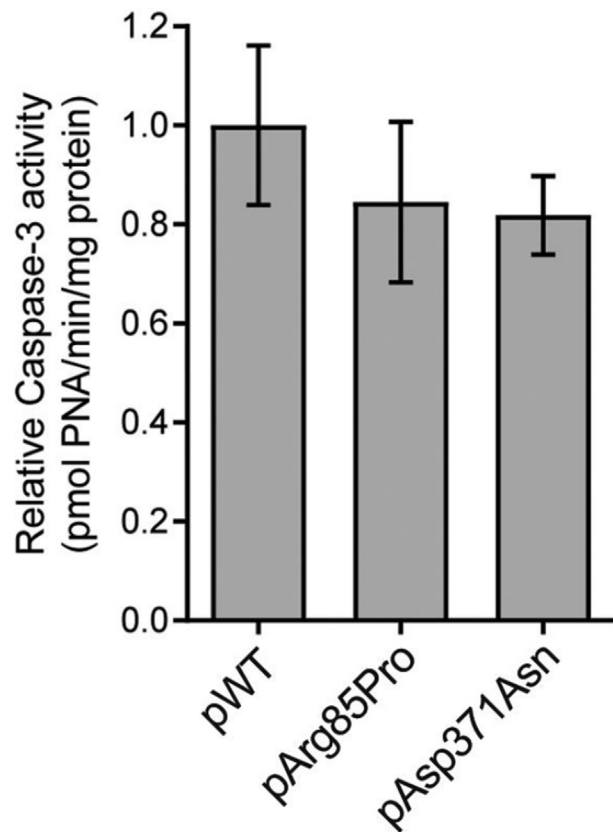
**Supplementary Figure 2.** Variant validation and segregation analysis. (A) c.1111G>A (p.Asp371Asn) *FAF1* variant in FAM13. Sequencing results show the heterozygous change in individuals III-3, III-5, IV-5, and IV-7. Sequencing results are shown using the reverse primer. The observed C>T heterozygous change corresponds to G>A in the forward orientation. (B) c.254G>C (p.Arg85Pro) *FAF1* variant in F-0681-00. Sequencing results show the G>C heterozygous change in the patient's sample. A reference sequence from a noncarrier is also presented.



**Supplementary Figure 3.** LOH results. LOH tested for 2 c.1111G>A (p.Asp371Asn) *FAF1* variant carriers (FAM13, individuals IV-7 and III-5). Results show a slight LOH in the tumor from patient IV-7 and a complete depletion of the wild-type allele in the case of the patient III-5.



**Supplementary Figure 4.** CRISPR/Cas9 *FAF1*<sup>KO</sup> modeling results. Time-course development of TRAIL-induced apoptosis, measured as caspase-3 activation (n = 1). On the right, representative images of treated cells at the indicated timepoints. Scale bar, 200  $\mu$ m.

*FAF1*<sup>KO</sup> 5

**Supplementary Figure 5.** Functional characterization of germline variants results. Determination of caspase-3 activity after TRAIL-induced apoptosis on *FAF1*<sup>KO</sup> 5. Cells expressing both p.Arg85Pro and p.Asp371Asn *FAF1* variants were more resistant to cell death in comparison to those expressing the wild-type form of *FAF1*.

**Supplementary Table 1.** PCR primers used in the study

	Forward	Reverse
FAF1 c.1111G>A	TCTTAGAATTTGATAGGCCAAAA	TTCTATTGCTGGACCCAAAG
FAF1 c.254G>C	GAAGAACAACACAAGCCAAGT	CCCTTCTTGCACTGGTAGTC

NOTE. Sanger validation of *FAF1* missense variants on patients' samples.

**Supplementary Table 2.** Mutation identification in replication cohort

FAF1	Forward	Reverse
FAF1_Ex1	CCAGACCAATCTTCCTGTCC	AACGCTGGGAAGAAGACTCC
FAF1_Ex2	GGTTGCCCATGAGAATCTTTGA	AGCTATGGTATGCTGAACCCA
FAF1_Ex3	CACACTTGGGCATTTATCTGTT	AGCTCTGTTCTTTGTTCTGCT
FAF1_Ex4	GAAGAACAACACAAGCCAAGT	CCCTTCTTGCCTGGTAGTC
FAF1_Ex5	AGTGTTAGCTCTGGATATGGACA	TTGCCAAATCTACTACTGCCA
FAF1_Ex6	TCTGTTTGTGTTGCTTCATGAG	TCCTTTCCCTTCAGTCAGAGA
FAF1_Ex7	AGCTAGAACTTGTTTCATCTCTGA	CCAACCAGAACAGATAAGCCC
FAF1_Ex8	CAGCCAGGAGTTGAAAACAAGA	GTGGCAAAAAGAGAAAGGAGGA
FAF1_Ex9	TTGGGCTCATACCAGTTTCC	TGGACAGTTTCTGCCTTCAA
FAF1_Ex10	CCTTCGGTCTACAGGTATCACA	ATTCTATTGCTGGACCCAAAGA
FAF1_Ex11	TGTGGGATTAGATGTTATGTGGT	CACAGTAGCATAAAACAGCATCA
FAF1_Ex12	AGACATTAGCCCCAACATTTACT	CAAATTCGTGAAGAGTTCATGT
FAF1_Ex13	GCTTTAGGAACTCCAAAATGTAAG	GCAACGAGCAGCTTTTGTCT
FAF1_Ex14	AACACAATGAGTTCTTTGTTGAAG	AAATATTGTCAGCTTGGGTGG
FAF1_Ex15	CTTCCGAAATTTCAACTGCC	CAAATTATTGGTCTTGGGG
FAF1_Ex16	TCCACTATGTACCATGCTGCT	AGCTTTCTCTATTGCAAACCCA
FAF1_Ex17	TGTGTTAAGTGCTTGTTCCTTTT	GGAAGGAAGGTAGGTTAACAGC
FAF1_Ex18	TCCCCACTCTCCATAGTCCA	CCTGCACCATGGGACTTTTC
FAF1_Ex19	TGCCTTGCAGGTTATTTTGA	GGAGGGTGGCAGAGTTGTAA

**Supplementary Table 3.** CRISPR Gene Editing

	Forward	Reverse
FAF1 sgRNA	CACCGTTCGACCTGTAATGCCATCC	aaacGGATGGCATTACAGGTCTGAAC
lentiCRISPR sgRNA cloning verification	GAGGGCCTATTTCCCATGATT	CCACTCCTTTCAAGACCTAGC
FAF1 gene editing verification	ATGGAGGTGAGACCATACCA	TGGCAGGAAAAACCTTACCA

**Supplementary Table 4.** Site-Directed Mutagenesis

	Forward	Reverse
FAF1 ORF c.1111G>A mutagenesis	GAAAGCCCGAaATAGAAAGCTTC	ACATAGAAGGCCTCTTAAAAAG
FAF1 ORF c.1111G>A sequencing	GGTGATTGCCATCCTGTATTT	TTGCTCTGTTGGAGTCCTTT
FAF1 ORF c.254G>C mutagenesis	TCAGCGTTTcACCTGTAATG	AGAAGAAGAGGAAGTAGG
FAF1 ORF c.254G>C sequencing	ATGGAGGTGAGACCATACCA	CCAACAGTACAGGTGTCTTCAA